Proceedings of the Sixth International Conference on
Railway Technology: Research, Development and Maintenance
Edited by: J. Pombo
Civil-Comp Conferences, Volume 7, Paper 20.2
Civil-Comp Press, Edinburgh, United Kingdom, 2024
ISSN: 2753-3239, doi: 10.4203/ccc.7.20.2

Optimizing Pearlitic Rail Steel Durability: Low-Temperature Annealing and Nanoscale Carbide Innovations

G. Tressia[1], L. H. Dias Alves[2], H. Goldenstein[3], C. R. Grandini[4], M. Mohtadi-Bonab[5] and M. Masoumi[6]

[1]ITV, Instituto Tecnológico Vale, Ouro Preto, Brazil
[2]Industrial Engineering Department, Federal University of Juiz de Fora, Brazil
[3]Department of Metallurgical and Material Engineering, University of São Paulo, Brazil
[4]Laboratório de Anelasticidade e Biomateriais, Universidade Estadual Paulista, Bauru, Brazil
[5]Department of Mechanical Engineering, University of Bonab, Iran
[6]Centro de Engenharia, Modelagem e Ciências Sociais Aplicadas, Universidade Federal do ABC, Santo Andre, Brasil

Abstract

This study investigates the impact of low-temperature annealing treatment at 200 degrees Celsius on the wear resistance and mechanical properties of eutectoid pearlitic steel, commonly used in railway applications. Our research primarily focused on understanding the microstructural changes and their correlation with mechanical hardness and wear resistance. Microhardness testing indicated that the hardness of the initial pearlitic microstructure increased from 370 HV to 400 HV following the low-temperature annealing treatment. This increase in hardness was linked to a substantial improvement in wear resistance, evidenced by a 27 percent decrease in wear rate. High-resolution Transmission Electron Microscopy analysis post-treatment revealed the emergence of nanoscale transition carbides. These needle-type transition carbides, with a hexagonal structure, contributed to an increased hardness of the pearlitic structure. Our findings suggest that the low-temperature annealing process not only enhances the hardness and wear resistance of pearlitic steel but also induces favourable microstructural changes that could significantly extend the service life of railway components.

Keywords: pearlitic steel, nanoscale carbide formation, wear resistance improvement, rail steel durability, rail, movable crossing.

1 Introduction

Railways, integral to global transportation due to their efficiency and safety, face increasing challenges as train speeds and axle loads grow. A key concern in this context is the durability of wheel and rail steels, particularly under the stresses of rolling contact fatigue (RCF) [1]. This fatigue often leads to significant material degradation and potential failure, posing serious operational and safety risks. In this environment, the performance of pearlitic steels, widely used in rail construction due to their strength and cost-effectiveness, is of paramount importance. The wear resistance of these steels is critical, especially as they are continually subjected to high-stress conditions. This resistance is not solely a matter of hardness but involves complex interactions at the microstructural level [2, 3]. As trains evolve to meet modern transportation demands, the need for more resilient railway materials becomes increasingly urgent. This study focuses on understanding and improving the wear resistance of pearlitic steel, aiming to extend the life and enhance the safety of railway components.

This study aims to rigorously examine and confirm the enhancement of wear resistance in pearlitic steel, a material extensively utilized in rail applications, through a novel low-temperature (200°C) heat treatment as proposed by Tressia et al. [7] in 2020. Despite extensive research efforts in metallurgy, achieving an optimal balance between hardness and toughness in pearlitic steel, particularly under the high-stress conditions experienced in railway environments, continues to pose a significant challenge. Our research hypothesizes that the formation of nanoscale transition carbides at this low temperature is instrumental in achieving substantial improvements in wear resistance. To substantiate this hypothesis, we have conducted a comprehensive set of microstructural analyses, including Scanning Electron Microscopy (SEM), Transmission Electron Microscopy (TEM), Selected Area Electron Diffraction (SAED), to verify the presence of these transition carbides. Additionally, we have correlated these microstructural changes with mechanical properties to elucidate their impact on the steel's wear and mechanical behavior. Our innovative approach seeks to bridge a critical knowledge gap in the field by demonstrating how the strengthening effects of nanoscale transition carbides can impede carbon migration and prevent the formation of brittle white etching layers, thereby enhancing the mechanical resilience of pearlitic steel. The low-temperature heat treatment method, validated through our extensive testing, is anticipated to not only improve wear resistance but also preserve rail integrity by avoiding embrittlement issues. The successful application of this treatment has the potential to significantly extend the durability of rails and other pearlitic steel components in railway systems, addressing a crucial need that has remained unfulfilled in prior academic endeavors.

2 Methods

Pearlitic rail steels with the chemical composition presented in Table 1 were subjected to heat treatment in an electric furnace at a temperature of 200°C for 30 min. The cooling was carried out in the air. Pins for wear tests were extracted from the rail

head, from rails with and without heat treatment, at a distance of 5 mm from the top to ensure a better microstructural homogeneity.

	C	Mn	Cr	Ni	Si	V	Mo	Fe
Rail steel (pin)	0.81	1.02	0.22	0.03	0.21	-	-	Bal.
H-13 steel (disc)	0.48	0.41	5.08	0.28	0.11	1.05	1.15	Bal.

Table 1. Chemical composition of the rail steel (pin) and H-13 steel (disc), wt.%

To assess the sliding wear of the specimens, we conducted laboratory tests using a pin-on-disc setup. Pins with a 5 mm diameter were derived from rail samples. Discs were fabricated with H-13 steel with a hardness of 600 HV; their chemical composition is detailed in Table 1. The choice of H-13 steel was informed by its robust thermal fatigue resistance, superior microstructural and hardness stability; it maintains its properties throughout the testing period, thereby effectively narrowing down the variables within the tribosystem. The sliding wear was set at a speed of 0.2 m/s, and the normal load was maintained at 100 N and the test was conducted for 60 min. Each condition was tested in triplicate. The friction force was measured during the test using a load cell. The coefficient of friction (COF) was obtained by the ratio between the friction force and normal load. Before and after the sliding wear tests, the samples were cleaned in an ultrasonic alcohol bath for 10 min, dried and weighed on an accurate electronic balance. The mass loss was obtained by the difference in mass of the samples before and after the tests. The dimensionless wear coefficient (K) of the pin was determined by the Archard wear equation, where Q is the volume worn per unit of sliding distance, W is the normal load and H is the hardness of the pin (softer surface of the tribosystem) [equation (1)].

$$Q = \frac{KW}{H} \qquad (1)$$

The volume worn of the pins was obtained by the ratio between the mass loss and the sample density (7.86 g/cm3). The microstructure and wear surfaces of the samples were examined using SEM. To measure the interlamellar spacing, we employed ImageJ software [11] on SEM images at a magnification of 50,000x. The microhardness was determined using the Vickers HV0.1 method, applying a test force of 0.980N. The measurement was repeated five times. The microstructural characterization of samples, both pre and post-heat treatment, was carried out using a transmission electron microscope (TEM - Tecnai G2-20 - FEI SuperTwin operating at 200 kV).

Dynamic Mechanical Analysis (DMA) was employed to obtain the internal friction spectrum of the samples with and without (as received) heat treatment. The used equipment was a Areva Metravib DMA-25 and samples with dimensions of 30×4×1 mm were used. The temperature range was between 150 K and 470 K, with a heating rate of 1 K/min.

Tensile tests were performed on both treated and untreated samples using an Instron model 3369 testing machine. In order to evaluate the structural integrity of the

rails following heat treatment, samples of 1.5-meter-long rails were subjected to a 4-point bending fatigue test. The tests were conducted in accordance with the standard EN 14587-1:2018 [13], which is used to evaluate welded rails. The application of the minimum and maximum cyclic loading was 110 kN and 450 kN, respectively, at a frequency of 5 Hz for a total of 2,000,000 cycles. The test was deemed successful if the sample withstood 2,000,000 cycles.

3 Results

A direct comparison of wear characteristics between the initial pearlitic and low-temperature annealed specimens is presented in Figure 1. The coefficient of friction (COF) trends (Figure 1a) for both as-received and annealed samples. Notably, the average COF was lower for the annealed samples (0.5±0.05) compared to the initial pearlitic structure (0.6±0.05). This difference is attributed to the increased hardness in the annealed samples, which reduces the frictional forces by mitigating adhesion and plastic deformation. Meanwhile, it is noted that microhardness test revealed that the hardness of the initial pearlitic microstructure increased from 370 ± 10 HV to 400 ± 15 HV following low-temperature annealing treatment at 200°C. Tressia et al. [7] also observed a similar trend, reporting a reduction in dislocation density in pearlitic rail steel post annealing at 200 ºC, which contributed to an improved deformation capacity.

Furthermore, the higher hardness of the annealed specimens effectively reduced the generation of wear debris and decreased the wear rate. This reduction is quantitatively demonstrated by a 27% decrease in wear rate and a lowering of the Archard wear coefficient (Figure 1b). These results collectively underscore the increased wear resistance imparted by the low-temperature annealing treatment, suggesting that such treatment induces beneficial microstructural changes, resulting in a material that is more robust and suitable for applications where wear resistance is crucial.

SEM images (Figure 2a and 2b) reveal the surface morphology of the as-received pearlitic specimen post-wear testing. This specimen, characterized by its inherently lower hardness, exhibited heightened susceptibility to wear. The SEM images show adhesion marks and material transfer (black arrows) and oxidized regions (blue arrows). The predominant wear mechanisms identified were plastic deformation, abrasion marks, and adhesion joint formation, which are attributed to the high contact pressure on asperities and the presence of hard abrasives, such as debris and oxides. EDS mapping (Figures 3c-e) underscores the significant presence of iron oxide on the specimen's worn surface. The sliding motion increased the accumulation of wear debris, intensifying the oxidation layer and contributing to material removal. This process resulted in a discontinuous oxide layer on the contact surface, which reduced direct metal-to-metal contact. Elevated temperatures from frictional heating were key in accelerating the formation of this oxide layer [14, 15]. Importantly, no direct correlation was found between the wear mechanism and mass loss. The observed adhesive wear manifested in the tearing and fragmentation of the worn surface, with asperities undergoing work hardening and eventually becoming wear debris.

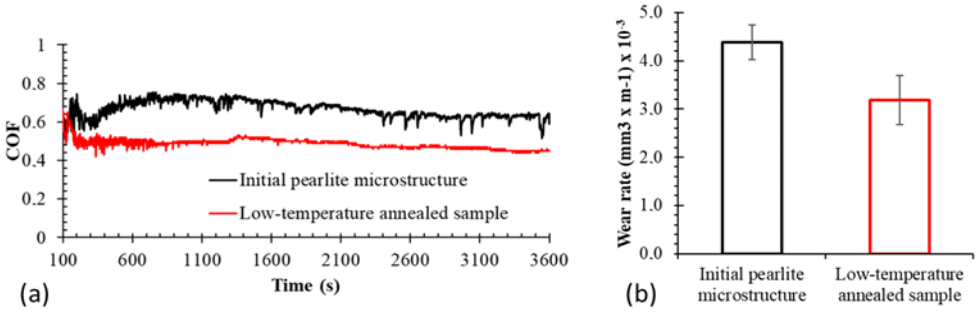

Figure 1: Comparison of COF (a) and wear rate (b).

SEM images (Figure 3a and b) reveal the worn surface of the low-temperature annealed specimen. Marked with black arrows, adhesion marks, adhesion joints, and material transfer are visible, while blue arrows highlight oxidized areas. Despite similar wear mechanisms to the as-received specimen, the annealed specimen exhibited enhanced wear resistance. This improvement is attributed to its increased hardness, which resulted in a reduced susceptibility to wear.

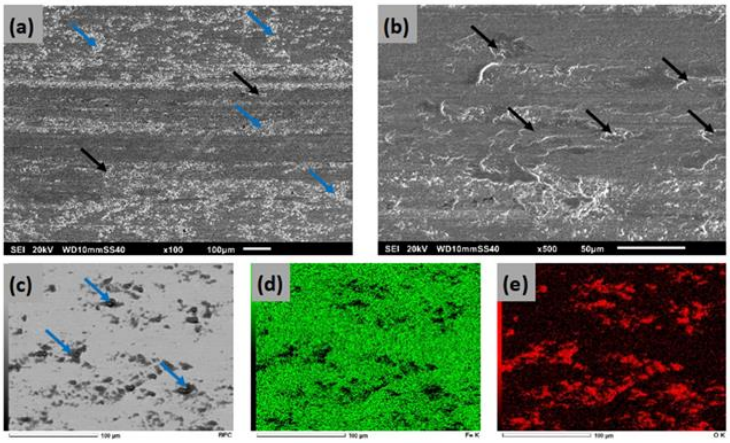

Figure 2: Worn surface of an as-received sample after the wear test observed by SEM (a) 100x, (b) 500x, (c) region of EDS mapping with backscattered electrons, (d) Fe mapping and (e) O mapping.

The formation of oxide layers on sliding surfaces within tribological systems presents a nuanced behavior towards the COF. These layers can increase the COF due to their inherent abrasive characteristics; however, a uniformly formed oxide layer might act as a protective barrier that minimizes metal-to-metal contact, thus potentially lowering the COF. This effect is particularly noticeable in specimens that have undergone low-temperature annealing, which likely promotes more consistent oxide layer formation and contributes to a lower COF. The adherence and integrity of these oxide layers are crucial as loosely bound layers may detach, increasing debris and adversely impacting the COF [16].

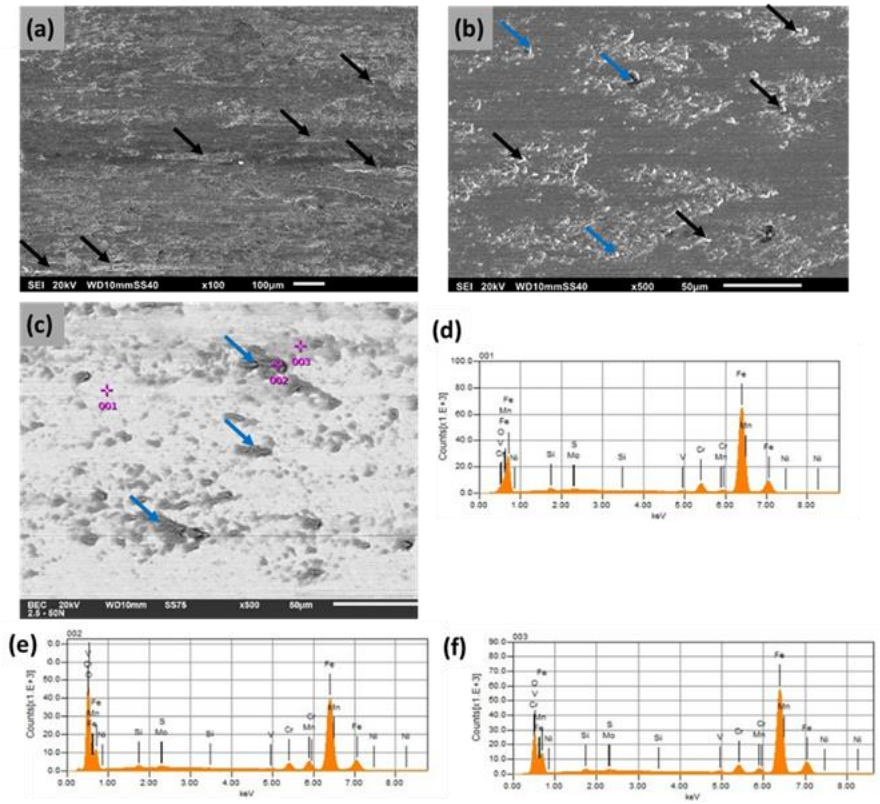

Figure 3. Worn surface of the low-temperature annealed specimen.

Figure 4 illustrates the engineering stress-strain curves for both the initial pearlitic and low-temperature annealed specimens. The annealed sample exhibited a yield strength increase of approximately 21% (from 720 ± 20 MPa to 875 ± 25 MPa), contrasted with a minor reduction in total elongation (from 12.1 ± 1.3 to 11.6 ± 1.5). This strength enhancement is primarily could be attributed to the formation of nanoscale epsilon carbides, identified in our TEM analysis, which also contribute to the slight decrease in ductility by impeding dislocation movement.

Resilience, measured as the area under the stress-strain curve up to the elastic limit, increased from 9.648 N.mm-3 in the initial pearlitic specimen to 10.172 N.mm-3 post-annealing, indicating an enhanced ability to absorb energy elastically. Additionally, the tensile fracture energy, representing the combination of material resistance and total elongation, remained consistent at around 105 ± 5.0 N.mm-3 for both specimens [17]. This consistency suggests that the low-temperature annealing improves strength without significantly compromising the material's overall toughness.

SEM micrographs in Figure 5a and 5b depict the microstructure of the as-received pearlitic steel, characterized by alternating lamellar patterns of ferrite (dark contrast) and cementite (bright contrast). This layered structure is crucial for the mechanical properties and wear resistance of rail steel, as they are highly influenced by interlamellar spacing and pearlite colony size [18–20].

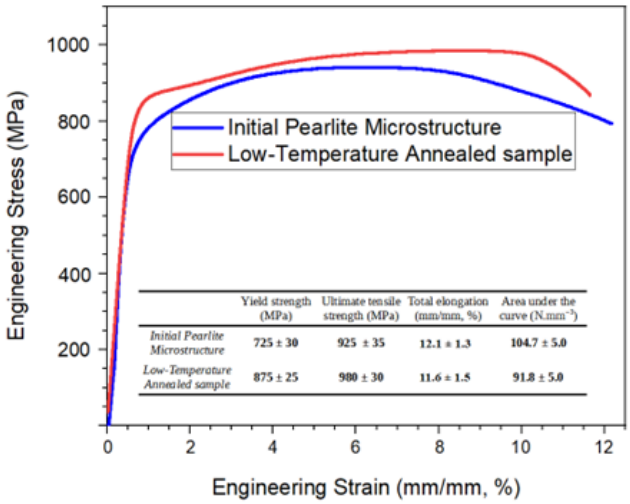

	Yield strength (MPa)	Ultimate tensile strength (MPa)	Total elongation (mm/mm, %)	Area under the curve (N.mm^{-2})
Initial Pearlite Microstructure	725 ± 30	925 ± 35	12.1 ± 1.3	104.7 ± 5.0
Low-Temperature Annealed sample	875 ± 25	980 ± 30	11.6 ± 1.5	91.8 ± 5.0

Figure 4: Engineering stress-strain curves of initial pearlite and low-temperature annealed specimens.

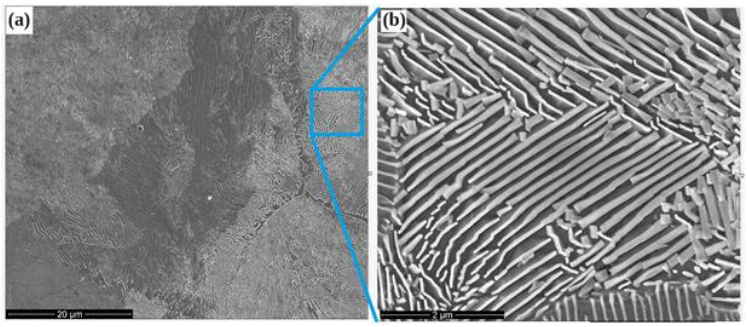

Figure 5: SEM micrographs of an as-received pearlitic specimen (a) and (b).

TEM images of an as-received pearlitic rail steel specimen are presented in Figure 6a and b, highlighting the distinct contrast between the soft ferritic matrix and the hard cementite. This contrast facilitates the identification of alternating lamellar ferrite and cementite layers. Pearlitic structures exhibit interlamellar spacing that can be reduced to less than 100 nm through accelerated cooling, compared to spacings greater than 200 nm following conventional air cooling in rail steels [23]. Figure 6c displays a microstructure of the as-received specimen, with electron diffraction patterns indicating the ferritic and cementite phases. The high carbon content of 6.68 wt% in the cementite phase is shown in Figure 9d and e. Diffusion eutectic transformation during heat treatment leads to a more homogeneous carbon distribution in the microstructure, resulting in more ductile cementite in the heat-treated specimen compared to the as-received specimen.

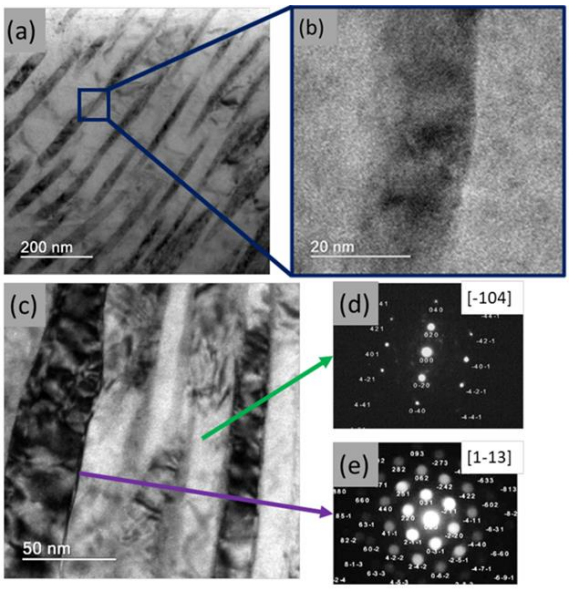

Figure 6. TEM images of the microstructure of an as-received (a) , (b) region highlighted in blue in (a) without transition carbides, (c) microstructure of other regions of the specimen, and diffraction patterns of the (d) NBD of ferrite region and (e) CBED of cementite.

SEM micrographs (Figure 8a and b) of pearlitic steel annealed at 200°C for 30 minutes reveal the characteristic ferrite and cementite lamellae colonies, showing no notable changes post-treatment. Low-temperature tempering is known to promote Cottrell atmosphere saturation and diminish solute carbon content through the gradual precipitation of transition carbides [33]. Krauss et al. [34] confirmed the precipitation of fine transition carbides during tempering between 150-200°C, which enhances mechanical resistance by limiting dislocation glide [35].

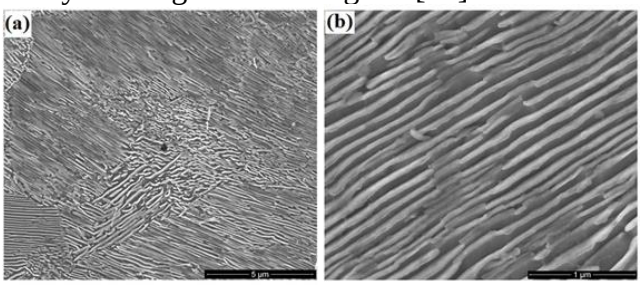

Figure 8: (a) and (b) SEM micrographs of pearlite heat-treated at 200°C for 30 min

High-resolution TEM images (Figure 9a-c) post heat treatment at 200°C for an hour highlight the emergence of nanoscale transition carbides, indicating the coexistence of ferrite and cementite. Particularly, Figure 9b shows these nanoscale carbides (marked by a black arrow), consistent with observations by Gutierrez et al. [36]**.** TEM analysis reveals needle-type transition carbides with a hexagonal structure, exhibiting a (001)α // (0001)carbide orientation relationship with the ferritic matrix. This crystallographic misfit might facilitate the formation of transition carbide precipitates by harnessing interstitial carbon atmosphere energy. Choi et al. [37] further elucidated the kinetics of this process, involving kink formations on screw

dislocation segments and pinning effects on edge dislocations, without significant recovery of the dislocation structure.

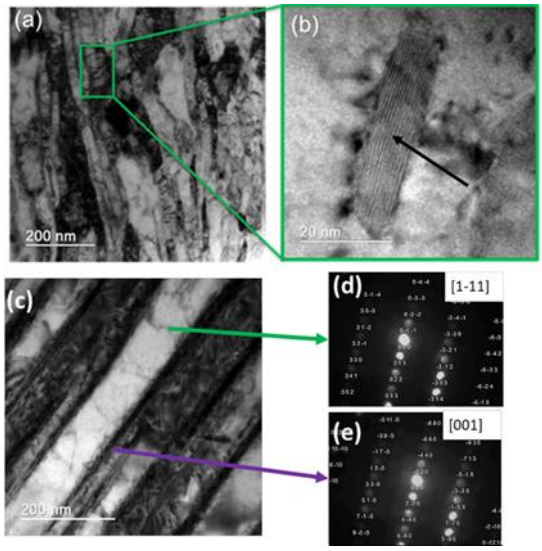

Figure 9. TEM micrographs of pearlite heat-treated at 200°C for 30 min. (a) microstructure of the treated region, (b) higher magnification of the region highlighted in green in (a), (c) another region with CBED diffraction patterns indicating (d) ferrite and (e) cementite.

Internal friction spectra measurement is a powerful technique for characterizing the mechanical properties and microstructure of materials. It can be used to detect and characterize carbide precipitation in a material by analyzing the energy dissipation of the material as it is subjected to a periodic stress or strain. As carbides precipitate, they can form discontinuities or inclusions within the pearlitic structure that can affect its mechanical properties [38, 39]. Carbide precipitation can cause a change in the internal friction spectra by creating additional sources of energy dissipation, which can be detected to determine the extent of precipitation. In addition, the temperature and frequency dependence of the internal friction spectra can provide information on the nature and distribution of the carbides within the material [40]. Interstitial solutes, such as carbon and nitrogen, can also affect the mechanical properties of steels by altering their lattice position in the vicinity of crystallographic defects. Figure 10 shows the Snoek peaks for both samples at these temperatures.

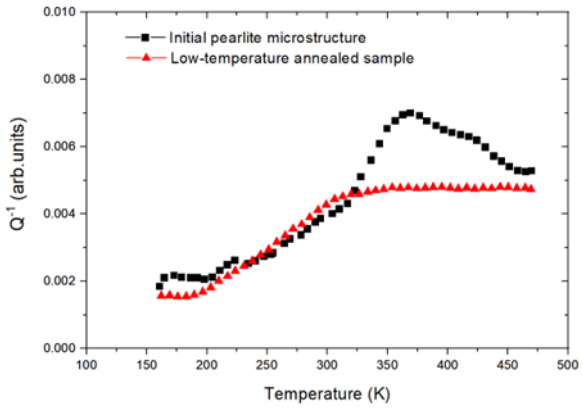

Figure 10: Internal friction spectra measured in investigated samples.

The peaks observed in the graph represent the energy dissipation associated with various types of defects or microstructural features, including dislocations, grain boundaries, and carbide precipitates. The position and intensity of these peaks can be utilized to extract information about the nature and distribution of these features within the material. Additionally, the frequency dependence of the internal friction spectra provides insights into the relaxation behavior of the material and the mobility of defects within it. For example, dislocation glides on <111> direction along (110) planes at room temperature in the BCC lattice, while kink-pair formation screw dislocations can also glide on (112) planes in the same <111> direction associated with the relaxation process by increasing the temperature from 100 °C [42, 43]. Figure 10 displays the internal friction curve of an as-received pearlitic sample, which exhibits a relaxation peak at ~370 K (~90 °C). This peak may be attributed to kink-pair formation on screw dislocation on both (110) and (112) planes coupled with stress-induced ordering of interstitial atoms [40, 41]. This peak disappears in treated samples, indicating the complete precipitation of C as carbide. These transition carbides may pin the dislocations and cause additional mechanical improvements in the resulting microstructure.

Upon low-temperature heat treatment at 200°C, our pearlitic samples underwent notable microstructural changes, mainly marked by the formation of nanoscale transition carbides from carbon redistribution. This evolution led to increased hardness, as these carbides impede dislocation movement, elevating resistance to deformation. While carbides typically possess higher stiffness than ferrite, the elastic modulus of our matrix slightly decreased post-treatment. This could be attributed to the localized strain fields at the carbide-ferrite interfaces, which subtly alter the material's overall stiffness. Thus, our findings underscore the intricate balance between microstructural changes and mechanical properties, emphasizing the nuanced interplay between hardness and elasticity induced by the low-temperature treatment.

Carbide precipitation notably influences the mechanical and wear properties of pearlitic steels. The morphology evolution, involving nanoscale transition carbides, provides intrinsic strengthening. These carbides resist plastic deformation onset, with their fine dispersion at key structural sites contributing to enhanced mechanical resilience. This results in higher hardness and improved sliding wear resistance.

The low-temperature heat treatment, aimed at improving the wear resistance of pearlitic steel rails, maintains structural integrity without inducing brittleness. To verify this, six rail samples, three treated and three untreated, each 1.5 meters in length, underwent a 4-point bending dynamic fatigue test over 2 × 106 cycles. All samples, regardless of treatment, passed the test without showing any signs of cracks or potential fractures. This outcome confirms that the heat treatment does not compromise rail safety and suggests significant benefits, such as increased rail durability, making it a promising option for wide-scale application in railway systems.

4 Conclusions and Contributions

The formation of nanoscale hexagonal transition carbides during low-temperature annealing at 200°C in pearlitic steel specimens is a critical factor in enhancing wear resistance. These carbides act as a strengthening mechanism, increasing hardness and

offering resistance to shear forces in sliding wear. This improvement is particularly significant for heavy haul railway systems, as it contributes to extending maintenance intervals by reinforcing rail durability under high-stress conditions.

The low-temperature heat treatment method maintains the structural integrity of the steel. Fatigue tests confirm that this treatment does not induce brittleness, ensuring the safety and reliability of rails. This feature is essential for the potential large-scale adoption of this treatment in the railway industry, providing a balance between enhanced performance and structural safety.

Acknowledgements

The authors gratefully acknowledge the support provided by CNPq, FAPESP, and Vale S.A.

References

[1] Liu C, Zhang G, Chen C, et al. Formation mechanism for the white etching microstructure in the subsurface of the failure pearlite wheel steel. Wear, 2022;494–495:204243.

[2] Fantecelle Strey N, Bavaresco Rezende A, da Silva Miranda R, et al. Comparison of rolling contact fatigue damage between railway wheels and twin-disc test specimens. Tribol Int, 2021;160:107037.

[3] Zhu H, Nguyen BH, Camacho ET, et al. Tribological behaviors of two distinct classes of white etching layers on rail surface. Wear, 2023;532–533:205097.

[4] Hieu Nguyen B, Al-Juboori A, Zhu H, et al. Formation mechanism and evolution of white etching layers on different rail grades. Int J Fatigue, 2022;163:107100.

[5] Hua J, Liu P, Zhang G, et al. Damage behavior and microstructure evolution of ER8C wheel steel under rolling wear conditions. Wear, 2022;510–511:204508. .

[6] Pan R, Chen Y, Lan H, et al. Investigation into the evolution of tribological white etching layers. Mater Charact, 2022;190:112076.

[7] Tressia G, Sinatora A, Goldenstein H, et al. Improvement in the wear resistance of a hypereutectoid rail via heat treatment. Wear. 2020;442–443:203122.

[8] Kimura T, Takemasa M, Honjo M. Development of SP3 rail with high wear resistance and rolling contact fatigue resistance for heavy haul railways. JFE Tech Rep. 2011;16:32–37.

[9] Tressia G, Sinatora A. Effect of the normal load on the sliding wear behavior of Hadfield steels. Wear, 2023;520–521:204657.

[10] Tressia G, Sinatora A, Goldenstein H, et al. Improvement in the wear resistance of a hypereutectoid rail via heat treatment. Wear. 2020;442–443.

[11] Stolze N, Bader C, Henning C, et al. Automated image analysis with ImageJ of yeast colony forming units from cannabis flowers. J Microbiol Methods, 2019;164:105681.

[12] ASTM E 1876-01. Dynamic Young's Modulus, Shear Modulus, and Poisson's Ratio by Impulse Excitation of Vibration. Annu B Am Soc Test Mater (ASTM), USA, 2012;i:1–16.

[13] Standard I. Irish Standard I.S. EN 14587-1:2018 Railway applications - Infrastructure - Flash butt welding of new rails - Part 1: R220, R260, R260Mn, R320Cr, R350HT, R350LHT, R370CrHT and R400HT grade rails in a fixed plant. p. 11.

[14] Neetu, Sangal S, Mondal K. Effect of various phase fractions of bainite, retained austenite, intercritical ferrite and pearlite on the wear behaviour of multiphase steels. Wear, 2022;500–501:204355.

[15] Hua J, Wu S, Zhang G, et al. Microstructure evolution and properties of wheel steel under different pearlite content and slip ratio conditions. Wear. 2023;512–513.

[16] Prates Ferreira de Almeida L, Entringer Falqueto L, Goldenstein H, et al. Study of sliding wear of the wheel flange - Rail gauge corner contact conditions: Comparative between cast and forged steel wheel materials. Wear, 2019;432–433:102894.

[17] Khedr M, Li W, Min N, et al. Effects of increasing the strain rate on mechanical twinning and dynamic strain aging in Fe-12.5Mn-1.1C and Fe–24Mn-0.45C–2Al austenitic steels. Mater Sci Eng A, 2022;842:143024.

[18] Saxena AK, Kumar A, Herbig M, et al. Micro fracture investigations of white etching layers. Mater Des, 2019;180:107892.

[19] Masoumi M, Echeverri EAA, Tschiptschin AP, et al. Improvement of wear resistance in a pearlitic rail steel via quenching and partitioning processing. Sci Rep. 2019;9:7454.

[20] Masoumi M, Loureiro R, Pinheiro P, et al. Effect of Pre-strain on Microstructure , Texture , and Strengthening of Fully Pearlitic Steel. J Mater Eng Perform. 2022;31:4642–4654.

[21] Aranda MM, Kim B, Rementeria R, et al. Effect of prior austenite grain size on pearlite transformation in A hypoeuctectoid Fe-C-Mn steel. Metall Mater Trans A Phys Metall Mater Sci. 2014;45:1778–1786.

[22] Benito S, Wulbieter N, Pöhl F, et al. Microstructural Analysis of Powder Metallurgy Tool Steels in the Context of Abrasive Wear Behavior: A New Computerized Approach to Stereology. J Mater Eng Perform. 2019;28:2919–2936.

[23] Tung PY, Zhou X, Mayweg D, et al. Under-stoichiometric cementite in decomposing binary Fe-C pearlite exposed to rolling contact fatigue. Acta Mater, 2021;216:117144. Available from: https://doi.org/10.1016/j.actamat.2021.117144.

[24] Zhou L, Bai W, Han Z, et al. Comparison of the damage and microstructure evolution of eutectoid and hypereutectoid rail steels under a rolling-sliding contact. Wear ,2022;492–493:204233.

[25] Kar'kina LE, Kabanova IG, Kar'kin IN. Strain Transfer across the Ferrite/Cementite Interface in Carbon Steels with Coarse Lamellar Pearlite. Phys Met Metallogr. 2018;119:1114–1119.

[26] Teshima T, Kosaka M, Ushioda K, et al. Local cementite cracking induced by heterogeneous plastic deformation in lamellar pearlite. Mater Sci Eng A [Internet]. 2017;679:223–229. Available from: http://dx.doi.org/10.1016/j.msea.2016.10.018.

[27] Zhang R, Wang J, Ma Y, et al. Sedimentary microfacies and palaeogeomorphology as well as their controls on gas accumulation within the deep-buried Cretaceous in Kuqa

Depression, Tarim Basin, China. J Nat Gas Geosci [Internet]. 2016;1:45–59. Available from: http://dx.doi.org/10.1016/j.jnggs.2016.04.003.

[28] Zhang L, Yang L, Sun K, et al. The Influence of Carbides on Atomic-Scale Mechanical Properties of Carbon Steel: A Molecular Dynamics Study. Nanomaterials. 2022;12:4179.

[29] Niessen F, Apel D, Danoix F, et al. Evolution of substructure in low-interstitial martensitic stainless steel during tempering. Mater Charact [Internet]. 2020;167:110494. Available from: https://doi.org/10.1016/j.matchar.2020.110494.

[30] Krbat'a M, Eckert M, Cíger R, et al. Physical modeling of CCT diagram of tool steel 1.2343. Procedia Struct Integr [Internet]. 2023;43:270–275. Available from: https://doi.org/10.1016/j.prostr.2022.12.270.

[31] Soliman M, Palkowski H. Tensile properties and bake hardening response of dual phase steels with varied martensite volume fraction. Mater Sci Eng A. 2020;777:139044.

[32] Ormsuptave N, Uthaisangsuk V. Modeling of bake-hardening effect for fine grain bainite-aided dual phase steel. Mater Des [Internet]. 2017;118:314–329.

[33] Järvinen H, Honkanen M, Järvenpää M, et al. Effect of paint baking treatment on the properties of press hardened boron steels. J Mater Process Technol. 2018;252:90–104.

[34] Krauss G. Steel: Processing, Structure, and Performance. Dairy Sci Technol CRC Taylor Fr Gr. 2014;Second Edi:1–542.

[35] Hutchinson B, Hagström J, Karlsson O, et al. Microstructures and hardness of as-quenched martensites (0.1-0.5%C). Acta Mater. 2011;59:5845–5858.

[36] Gutierrez I, Aranzabal J, Castro F, et al. Homogeneous formation of epsilon carbides within the austenite during the isothermal transformation of a ductile iron at 410 °C. Metall Mater Trans A. 1995;26:1045–1060.

[37] Choi WS, Lee J, De Cooman BC. Internal-friction analysis of dislocation-interstitial carbon interactions in press-hardened 22MnB5 steel. Mater Sci Eng A. 2015;639:439–447. Available from: http://dx.doi.org/10.1016/j.msea.2015.05.055.

[38] Sedmák P, Seiner H, Sedlák P, et al. Application of resonant ultrasound spectroscopy to determine elastic constants of plasma-sprayed coatings with high internal friction. Surf Coatings Technol. 2013;232:747–757.

[39] Magalas LB. Mechanical spectroscopy, internal friction and ultrasonic attenuation: Collection of works. Mater Sci Eng A. 2009;521–522:405–415.

[40] Golovin IS, Cordero F. 19th International Conference on Internal Friction and Mechanical Spectroscopy. J Alloys Compd ,2021;856:157688

[41] Vandewalle L, Konstantinović MJ, Verbeken K, et al. A combined thermal desorption spectroscopy and internal friction study on the interaction of hydrogen with microstructural defects and the influence of carbon distribution. Acta Mater. 2022;241:118374.

[42] Lilensten L, Couzinié JP, Perrière L, et al. Study of a bcc multi-principal element alloy: Tensile and simple shear properties and underlying deformation mechanisms. Acta Mater. 2018;142:131–141.

[43] Ventelon L, Caillard D, Lüthi B, et al. Mobility of carbon-decorated screw dislocations in bcc iron. Acta Mate, 2023;247:118716.

[44] Martin R, Mari D, Schaller R. Influence of the carbon content on dislocation relaxation in martensitic steels. Mater Sci Eng A. 2009;521–522:117–120.

[45] Zubkova TA, Yakovleva IL, Kar'kina LE, et al. Study of the Hardness and Elastic Modulus of Cementite in the Structure of Granular Pearlite by the Nano-Indentation Method. Met Sci Heat Treat. 2014;56:330–335.

[46] Zhao L, Wang Q, Shi G, et al. In-depth understanding of the relationship between dislocation substructure and tensile properties in a low-carbon microalloyed steel. Mater Sci Eng A [Internet]. 2022;854:143681.

[47] Wiengmoon A, Pearce JTH, Nusen S, et al. Electron microscopy study of carbides precipitated during destabilization and tempering heat treatments of 25 wt.%Cr-0.7 wt.%Mo high chromium cast irons. Micron, 2021;143:103025.

[48] Geng B, Liu Z, Li Y, et al. Analysis of evolution law and mechanism of stacking fault density of M7C3 carbides under the action of the electric current pulse. Mater Charact, 2022;191:112117.

[49] Gorunov AI. Investigation of M7C3, M23C6 and M3C carbides synthesized on austenitic stainless steel and carbon fibers using laser metal deposition. Surf Coatings Technol, 2020;401:126294.